Austin Gurley[1]
Department of Mechanical Engineering,
Auburn University,
1418 Wiggins Hall,
Auburn, AL 36849
e-mail: arg0007@auburn.edu

David Beale
Professor
Department of Mechanical Engineering,
Auburn University,
1418 Wiggins Hall,
Auburn, AL 36849
e-mail: bealedg@auburn.edu
Mem. ASME

Royall Broughton
Professor Emeritus
Department of Polymer and
Fiber Engineering,
Auburn University,
115 Textile Building,
Auburn, AL 36849
e-mail: brougrm@auburn.edu

David Branscomb
Research Specialist
Composite Structures,
Takata Highland,
1350 Bridgeport Drive, Suite 1,
Kernersville, NC 27284
e-mail: david.branscomb@takata.com

The Design of Optimal Lattice Structures Manufactured by Maypole Braiding

Beginning with the maypole braiding process and its inherent constraints, we develop a design methodology for the realization of optimal braided composite lattice structures. This process requires novel geometric, mechanical, and optimization procedures for comprehensive design-ability, while taking full advantage of the capabilities of maypole braiding. The composite lattice structures are braided using yarns comprised of multiple prepreg carbon fiber (CF) tows that are themselves consolidated in a thin braided jacket to maintain round cross sections. Results show that optimal lattice-structure tubes provide significant improvement over smooth-walled CF tubes and nonoptimal lattices in torsion and bending, while maintaining comparable axial stiffness (AE).
[DOI: 10.1115/1.4031122]

Introduction

The formidable cost of high-performance fiber composites is aggravated by the required labor-intensive and high material costs of their manufacturing processes. Manufacturing techniques which are automated and which minimize material scrap can greatly aide in this concern. Braiding of near-net-shape composite preforms offers a mechanized and material-efficient solution to these concerns in many cases [1]. In a composite structure, it is desirable to place reinforcement in locations that can contribute most to stiffness or strength for efficient use of material.

Maypole braiding is a weaving method that uses meshed gears arranged in a circle to carry packages of yarn in interlacing patterns; this arrangement is particularly suited for producing circular fabrics (Fig. 1). We intend to show that many shapes—geometrically suitable for high stiffness and strength—can be made with this machine. More complex and costly three-dimensional computer-controlled braiding machines and some lace braiding machines are capable of creating more complex shapes; however, the machines themselves often are quite expensive and produce parts at low production rates [2,3]. It is therefore desirable to study the extent to which a traditional braiding machine can manufacture a "designed" composite [4]. By braiding tows of carbon pre-impregnated with epoxy, a braided lattice can be formed, which becomes a rigid structure upon curing. Tows of different sizes can be combined to form lattice elements of various sizes for reinforcement within different portions of the structure.

The approach taken here is specific to beams, shafts, beam-columns, and truss members, as might be purchased commercial off-the-shelf. Rather than make tubular members with smooth walls without holes, this research focuses on the use of standard braiding machinery and methods to create a lattice braid to improve strength/weight ratios. Improving strength-to-weight ratios is important in minimal weight design, where the term "specific stiffness" is used to mean stiffness per unit mass or modulus per unit density [5]. When engineering fibers and structures made thereof, traditional density (kg/m^3) is often not a useful

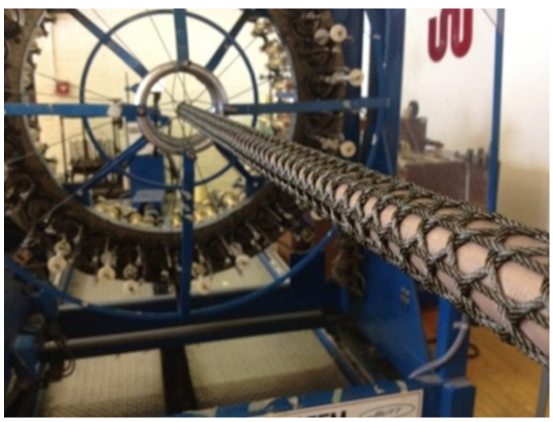

Fig. 1 Maypole braiding open-structure composites

[1]Corresponding author.

Contributed by the Design Automation Committee of ASME for publication in the Journal of Mechanical Design. Manuscript received February 10, 2015; final manuscript received July 15, 2015; published online August 6, 2015. Assoc. Editor: Nam H. Kim.

concept since it must be derived using the structure's cross-sectional area which is often difficult to accurately measure. Typically linear density (kg/m) is used instead. In the design of beams and shafts, stiffness per unit linear density is the important specific stiffness with units $\mathrm{N \cdot m/kg}$ for axial loading and $\mathrm{N\,m^2/kg}$ in bending and torsion. Prior relevant work in braiding includes the development of high-performance tethers and the development of a lattice truss that requires manual secondary interlacing after machine processing [6]. No rigid lattice structures have yet been fabricated without such significant manual intervention or complex 3D braiding machinery [6]. This article presents the development of three computational models: geometry, mechanics, and optimization tools for the design of braided open-structures.

Many braid geometry models have been explored in equations or finite element (FE) form. Most existing analytical models are concerned with fabrics that have very fine fibers [1,7–9]. While useful for many preforms, these fiber models are not capable of producing the large undulations found within the lattice tubes when composite yarns intersect or interlace at joints (as shown later in Fig. 3). Other simulations have been created, which directly calculate dynamically the exact motions and geometry of a braiding machine and the interlacing of the yarns onto a surface [10–12]. While capable of solving for large yarns, the simulation requires intensive computation using dynamic FE models [13]. The kinematics of the braiding machine motion has been explored, but not developed in a general parametric manner [4].

Mechanics modeling for subsequent optimization should provide a computationally efficient simulation that adequately represents the geometry and structural fidelity of the open structure. It is visually evident that the carbon composite yarns and the intersection of carbon yarns forming the joints create a space-frame structure. This form of structure is most easily represented using "beam" FE [14]. The element formulations useful to this work for space frames have been derived from multiple sources [15,16].

Significant and copious research in structural optimization has led to the realization that the optimal shape to minimize the weight of structures is a space frame—by loading the elements primarily in tension and compression, the material strength is fully utilized [17]. In this work, sizing optimization techniques are employed [18–20]. The objective is to maximize the specific stiffness of the entire structure by (formally) minimizing its compliance. The design variables requiring optimization are chosen in this work to be the individual yarn cross-sectional areas within the braid. Compliance minimization allows each yarn's relative contribution to structural stiffness to be determined, and the yarn diameters updated accordingly, using the optimality criteria (OC) method, which is well-suited for large structure finite-element analysis (FEA) problems [20]. This work optimizes the structure using conventional methods but includes the special constraints of the braiding process.

This article presents aspects of geometry, mechanics, and optimization of braided lattices. Geometric modeling with machine parameterization is used to create an interlaced form based on the machine kinematics. This model includes the effects of machine geometry and interyarn tension during braiding. It is discretized into nodes between short segments in the modeling process. An assembly of beam FEs is built directly from the resulting geometry model nodes for mechanical simulation. Appropriate material properties are given to these beam elements. This mechanical model is compared to physical test data and is shown to accurately predict structure stiffness for a test geometry. A sizing optimization algorithm predicts optimal braided lattice geometries under known loads, using OC. Finally, resulting lattice-structure tubes' mechanical properties are compared to full-walled commercial products.

Open-Structure Braiding Process

The braiding process involves simultaneous motions of several machine parts (Fig. 1). Two sets of spring-loaded *carriers*—each bearing spools of yarns to be braided—are passed in opposite directions between *horn gears* and made to travel around a *track plate*. As the carriers follow their sinusoidal paths, they release *yarn* from spools wound with nearly uniform tension. These yarns interlace each other and are pulled down toward the *fell-point* where they meet and become a *preform* fabric. Typically the yarns form against a *mandrel*, which is pulled away from the machine at a known speed to control the braid helix angle. The mandrel cross section can be nearly any convex shape; it is typically circular such that the preform is cylindrical. The braid also allows the inclusion of a third axis of yarn (in addition to clockwise and counterclockwise), which is laid down axially along the braiding path.

In the present work, the braided yarns consist of a prepreg carbon tow core inside a thin braided jacket, as described in a previous article [4]. The prepreg carbon core provides rigid structure upon curing. The braided jacket bundles multiple tows of carbon filaments together, allowing easy variation of yarn size and constraining the yarn to maintain a round cross section during braiding. The yarn jacket typically consists of materials much softer than the carbon core (such as nylon); thus, measuring a yarn's stiffness and dividing by the cross section to retrieve a "modulus" is not very consistent. The most accurate method is simply to measure and assign axial, bending, and torsional stiffness to the beam (yarn) based on physical testing of the yarn. The relevant properties are axial stiffness (AE), flexural stiffness ($E_{(\mathrm{flex})}I$), and torsional stiff (JG). Intrinsic properties (moduli E, E_{flex}, and G) could be derived from these values if desired.

The bonded yarn intersections physically consist of two or three overlapping yarns, with a thin film of resin between them. It has been found through physical testing that the strength of joints does not vary significantly with yarn diameter. The joint intersection will be given the effective properties of this bonded joint, different from those of the yarns themselves.

Geometry Model

An accurate geometry model of the final braided structure begins by determining the controlled variables in the braiding process. Some of these are limits of the maypole braiding process while others are limited based on the particular machine being used. The variables needed to fully describe a braid are given in Table 1.

These few parameters can describe the motion of yarn carriers on the braider. It is seen in the track-plate geometry that the carrier path is a sinusoid superimposed on a circle (Fig. 2). The motion requires only one parametric equation for the radius, and a transformation applied to it for rotation around the circle. Traditionally each horn gear has four radially directed slots spaced 90 deg apart; two adjacent slots are occupied by carriers at any instant. Consideration of these interactions leads to the following

Table 1 Braid geometry design variables

Variable and symbol	Example value
Counting variables	
Parameter, t	Parameter variable
Yarn location in space, X_n^a, Y_n^a, Z_n^a or R_n^a, θ_n^a, Z_n^a	N/A
Carrier position # $[\cdot]_n$	Varies from 1 to g
Yarn location $[\cdot]^a$	Warp, weft, axial
Machine/braid dimensions	
Machine diameter, D (m)	0.06
Mandrel diameter, d (m)	0.0445
Horn gear diameter, Θ (m)	0.01
Helix angle, ψ (deg)	45
Pitch (m)	0.1396
Yarn diameter, Δ (m)	0.002
Total horn gears, g	32
No. of horn gear slots, f	4

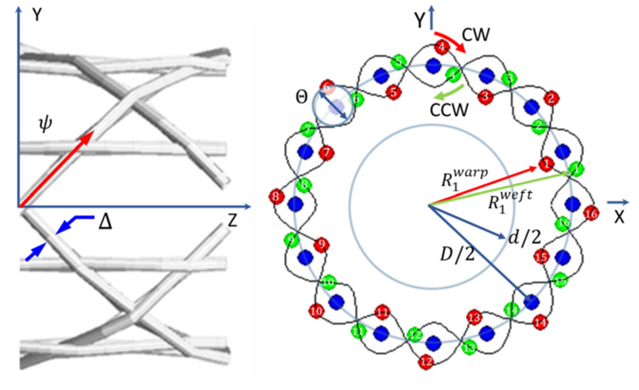

Fig. 2 Kinematic equations replicate braiding machine motion from key machine variables

newly developed parametric expression for the radius of the carrier path for an arbitrary machine construction:

$$R_n^{\text{warp}} \equiv \frac{\Theta}{2} \times \cos\left(\frac{g}{2}\left(t - \frac{n\pi}{fg}\right)\right) + D/2 \tag{1}$$

Note that the position is shifted based on which number n of the g carriers is of interest and the number of slots (or "forks") f in each horn gear. The path of the weft carriers is found similarly, but must account for a phase shift (the reason carriers do not crash at horn gear intersections)

$$R_n^{\text{weft}} \equiv -\frac{\Theta}{2} \times \cos\left(\frac{g}{2}\left(t - \frac{n\pi}{fg} + \frac{(2f-1)\pi}{g}\right)\right) + D/2 \tag{2}$$

The path of the warp carriers in Cartesian coordinates is simply the transformation of R and an angular displacement that is a function of the parameter t

$$X_n^{\text{warp}} = R_n^{\text{warp}} \times \cos\left(-t - \frac{n\pi}{fg}\right) \tag{3}$$

$$Y_n^{\text{warp}} = -R_n^{\text{warp}} \times \sin\left(-t - \frac{n\pi}{fg}\right) \tag{4}$$

Corresponding expressions for the weft carriers are derived

$$X_n^{\text{weft}} = R_n^{\text{weft}} \times \cos\left(t + \frac{n\pi}{fg} - \frac{(2f-1)\pi}{g}\right) \tag{5}$$

$$Y_n^{\text{weft}} = R_n^{\text{weft}} \times \sin\left(t + \frac{n\pi}{fg} - \frac{(2f-1)\pi}{g}\right) \tag{6}$$

The paths these equations create mimic the track-plate shape and carrier motion, as seen in Fig. 2.

As a final step, each yarn is carried upward in the Z direction linearly as t increases. The wrapping (helix) angle ψ is related to the yarn helical pitch through the expression

$$Z_n^{\text{warp}} = Z_n^{\text{weft}} = \frac{2t}{g} \times \text{pitch} = \frac{2\pi D t}{g}\tan(\psi) \tag{7}$$

Axial yarns are modeled simply as vertical lines centered above their respective horn gear locations. Equations (1)–(7) describe the kinematic representation, as rendered in Fig. 3(*a*).

Open-structure braid is formed around a mandrel in production. The combination of tension due to the carriers and wrapping around the mandrel pulls the structure tight against the underlying mandrel shape. Because the kinematic model was based on the sinusoidal motion of the machine, it does not include this compressive effect. The effect can be created without unnecessary complexity of a dynamic simulation. This is accomplished in three steps: discretization, compression, and tension.

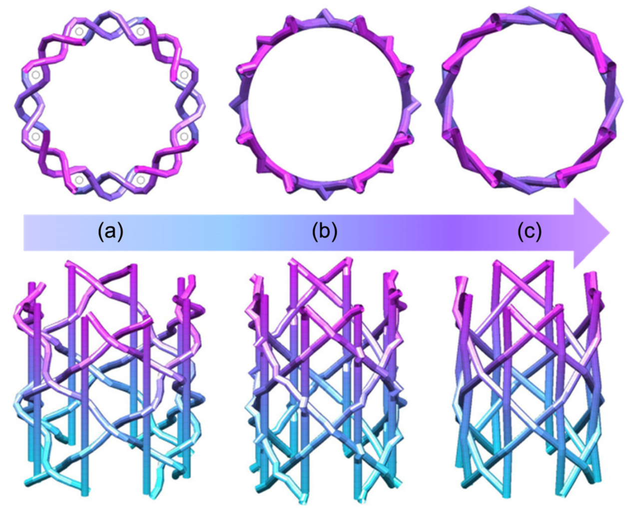

Fig. 3 Three stages of the geometry modeling process: (*a*) kinematics, (*b*) compression, and (*c*) tension

First, each overlap of yarns is sorted and identified. Yarn paths are discretized into short segments. The segments will later define the beam elements of the mechanical model. It is ensured that segment nodes lie normal to yarn overlapping "joints."

Next, joints are compressed against the mandrel as closely as possible while preserving the stacking sequence at each. Each yarn is considered independently with respect to its unique path on the mandrel and contact with its interlacing partners. The results of the artificial compression are shown in Fig. 3(*b*).

The artificial compression model is a significant improvement over the machine kinematics model and represents well a structure which has been pressed against a mandrel by vacuum bag or other means. However, typically the final laid yarn geometry is determined by tension within the yarns during braid formation. Again, this could be solved using contact FE methods, but an artificial method is computationally more attractive. The path taken by tensioned string or yarn is a geodesic, or shortest path, from one end to the other under load. This is a property of all strings and cables in tension. Interyarn tension is modeled by minimizing the free length of the yarns in the model while maintaining interlacing and mandrel contact constraints. The results are shown in Fig. 3(*c*). Notice the much improved replication of axial yarn undulation and the ability of the helical yarns to transition from straight to curved as they intersect with the mandrel. Thus, a realistic computational model of the braid geometry has been achieved.

Mechanical Modeling

The mechanics model should provide a computationally efficient simulation that adequately represents the geometry of the open structure, the CF yarns which constitute the bulk of the material, and the intersection of carbon yarns at joints that connect the carbon yarns. The analysis must also incorporate a method for easy application of the beam loads (uniaxial tension and compression, bending and torsion) and constraints. The loads and constraints will be applied only to the ends of the structure as is the case for struts, columns, and shafts in practice.

Each single cured yarn in the structure is supported by the joint intersections at regular intervals. This distance between supports (i.e., yarn intersections) is long compared to the diameter of the yarn; thus, it is assumed that the free-standing length of each yarn can be accurately modeled as a beam. A major benefit of the beam model is the easy incorporation of experimental yarn stiffness and strength properties. In certain situations, the yarns paths are straight and simply modeled as a straight beam between nodes created in the geometry modeling process. The straight element formulation uses Timoshenko shear-corrected beams [15]. A curved beam formulation is used in those places where the yarn lies against the curved mandrel surface [16].

Because they represent epoxy bonding, the intersection of joints should have different properties than those of the yarns themselves. Intersections are thus modeled as straight and short beam elements (Fig. 4), with stiffness and strength properties taken from physical testing of the bond between the composite yarns. Geometry and material parameters for an actual CF open-structure construction are presented in Table 2.

Validation

The model is now validated by comparing predicted stiffness and mass to a physical sample of a typical lattice structure. The structures can be made in many configurations: Figure 5 shows configurations of some of the main design parameters. The first structure shown is a basic true triaxial [6]: eight axial yarns, four warp, four weft, and a 45 deg helix angle. The structure can be modified in several ways. First, helical yarns could be added to the basic structure. Alternately, axial yarns could be added or removed. Yet another alternative is to keep the yarn count the same as the basic structure, but to change the helix angle. Any combination of these is also valid.

The physical sample tested was of the same geometry as the "base true triaxial" described in Table 2 and shown in Fig. 5. Five specimens were fabricated, weighed (to find mass/length), and tested in axial compression (to find structure AE), bending (EI of structure), and torsion (JG of structure). The model matches the experiment within the first standard deviation of physical testing data (Table 3). More results of the tests, both physical and computational, are detailed by Gurley [22]. Manufacturing inconsistencies are believed to be the primary cause of the variance and may be improved with better braiding equipment (machines designed for higher tension braiding) and quality control.

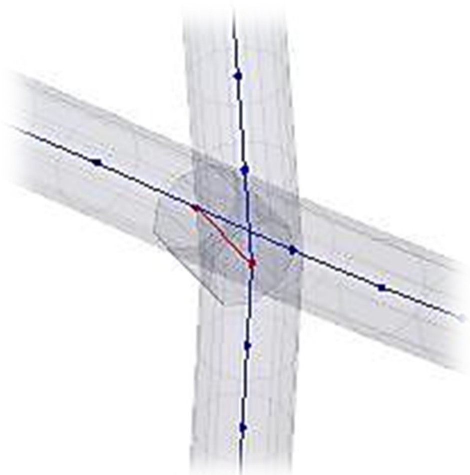

Fig. 4 Example of joint-intersection beam elements

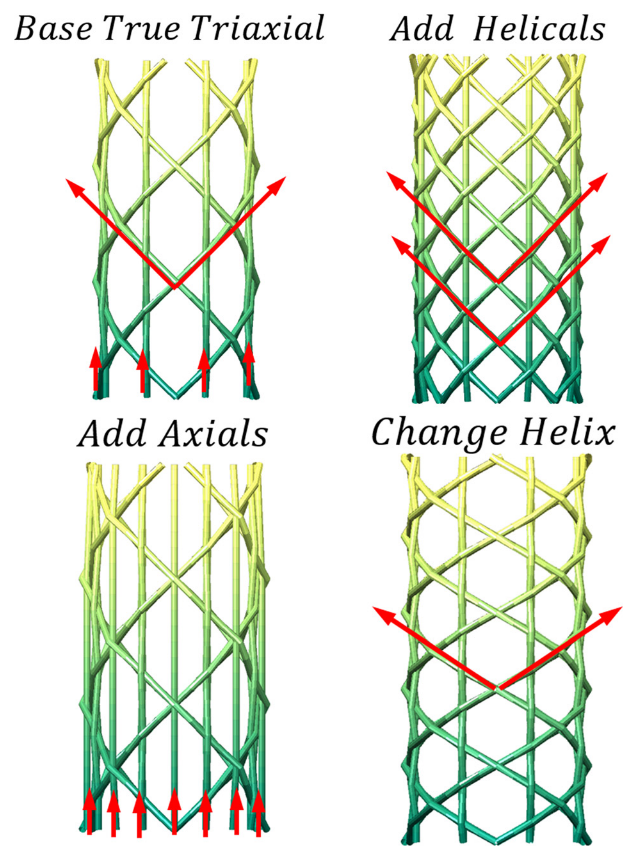

Fig. 5 Major design variables of the optimal braided lattice structure. The base true triaxial sample was manufactured for model validation.

Table 2 Construction geometry and material parameters specifications

Experimental braid geometry		Material model	
Mandrel diameter (mm)	31.8	Yarn AE (kN)	23.7
Helix (deg)	45	Yarn JG (N m^2)	1.5
No. of warp yarns	4	Yarn EI (N m^2)	80
No. of weft yarns	4	Mean diameter (mm)	2.3
No. of axial yarns	8	Linear density (g/m)	1.40
Height (cm)	100.0	Joint AE (kN)	123
Pitch (cm)	9.97	Joint EI (N m^2)	0.06
No. of gears g	32	Joint JG (N m^2)	0.12

Table 3 Results of the validation experiment

	AE (N)	JG (N m^2)	EI (N m^2)	M/L (g/cm)
Experimental	1220.8	384.0	138.4	1.200
(first standard deviation)	(176.5)	(55.5)	(20.0)	(0.037)
Model results	1228.0	357.9	139.6	1.205
(% error)	(0.6)	(−6.8)	(0.9)	(0.4)

Optimization

The present objective is to apply established sizing optimization techniques within the special constraints imposed by the braiding process to create high specific stiffness structures. It was found during the FE development previously that open-structure efficiencies are always improved by the increase of mandrel diameter; thus, the design diameter should be as large as the application allows. In the first step of optimization, the ideal helix angle ψ is determined by unconstrained optimization using a sweep of helix angle as the single design variable in FEA, with the objective of minimizing structure compliance. The primary optimization process now focuses on determining the carrier loading positions on the braiding machine and diameters of the yarns. The complete optimization process follows the following outline:

(1) Choose a machine and its inherent constraints such as number of yarns, maximum yarn diameter, etc.
(2) Choose the largest mandrel diameter possible for the design application.
(3) Model a structure with all yarns as large as possible and loaded on the machine of step #1 and using diameter from step #2.
(4) Perform unconstrained optimization of helix angle.
(5) Find the yarns which contribute least to structural stiffness and decrease their diameter a small amount. Find the yarns which contribute most to structural stiffness and increase their diameter a small amount (up to the max size allowed).
(6) Model the new structure with modifications suggested by step #5. Repeat step #5 until the solution converges.

The remainder of this description of optimization focuses on the complexity and proper mathematical treatment of step #5.

The formal optimization statement is

$$\left\{\begin{array}{ll} \min_x: & c(\boldsymbol{\delta}) \equiv \mathbf{U}^{\mathrm{T}}\mathbf{K}\mathbf{U} = \sum_{i=1}^{N_s}\sum_{e=1}^{N_y} u_{e,i}^{\mathrm{T}} k_{e,i} u_{e,i} \\ \text{subject to}: & \dfrac{V(\boldsymbol{\delta})}{V_0} = \nu \\ \mathbf{K}\mathbf{U} = \mathbf{F} & \\ 0 < \delta_{\min} < \boldsymbol{\delta} < \delta_0 & \end{array}\right\} \tag{8}$$

All driving equations are expressed in terms of the design variable $\boldsymbol{\delta}$, the vector of all yarn-diameters-squared (the reason for this choice of design variable is explained in the subsequent paragraph). The objective is to minimize the external energy or "compliance" $c(\boldsymbol{\delta})$. This objective is limited by a volume fraction equality constraint that specifies final volume $V(\boldsymbol{\delta})$ as a fraction ν of the initial volume V_0. The solution is also constrained to valid FE solutions $\mathbf{KU} = \mathbf{F}$ and to acceptable yarn-diameters-squared. The global structural load vector, global stiffness matrix, and global deformation matrix are denoted $\mathbf{F}$, $\mathbf{K}$, and $\mathbf{U}$, respectively. All loads $\mathbf{F}$ are applied to the single control node at one end of the structure—the other end is fixed. Each beam element has a local stiffness matrix $k_{e,i}$ and deformation vector $u_{e,i}$. The subscript i counts yarns from yarn number one to the total number of yarns in the structure, N_s. The subscript e counts beam elements along each yarn, from the first-most element to the end-most element in the yarn, element N_y. The sum of individual element compliances ($u_{e,i}^{\mathrm{T}} k_{e,i} u_{e,i}$) is equal to the global compliance ($\mathbf{U}^{\mathrm{T}}\mathbf{K}\mathbf{U}$).

This particular application of sizing optimization to braided trusses has two variations from the typical approach. First, in the braided structure, there is no need to penalize yarns with intermediate diameter in general, i.e., there is no reason to force yarn diameters Δ_i to maximum or minimum limits, as all yarn sizes can be fabricated equally easily. Also, yarns should have a constant Δ_i along their entire length (l_i); so, although each yarn is composed of many beam elements along its length, they are specified to be of equal diameter. The objective is formulated and grouped to reveal the yarnwise compliances

$$c(\boldsymbol{\delta}) \equiv \mathbf{U}^{\mathrm{T}}\mathbf{K}\mathbf{U} = \sum_{i=1}^{N_s}\sum_{e=1}^{N_y} u_{e,i}^{\mathrm{T}} k_{e,i} u_{e,i} \tag{9}$$

When choosing the design variables, it is desirable for the objective function to be linear in the design variables to ensure efficient convergence [19]. Unfortunately k_i is not sufficiently linear in Δ_i ; the AE of the yarn is proportional to Δ_i^2, while bending and torsional stiffness are proportional to Δ_i^4. To implement OC method, the design variables are transformed by using the square of diameter

$$\delta_i \equiv \Delta_i^2$$

This is dimensionally similar to regarding the cross section area as the design variable, as commonly used in truss optimization work [20]. If it is assumed that the AE of the yarn is significant compared to its bending and torsional stiffness, then the nonlinear terms in $k_i(\delta_i)$ are relatively small which facilitates rapid convergence.

Each yarn's *relative* contribution to structural stiffness is found using the OC method [20,23] by determining each yarn's value contribution toward compliance ($\partial c_i/\partial \delta_i$) and volume ($\partial V/\partial \delta_i$). The response of yarn compliance to a change in ρ_i

$$\frac{\partial c_i}{\partial \delta_i} = \sum_{e=1}^{N_y} -u_{e,i}^{\mathrm{T}} k_{e,i} u_{e,i} \tag{10}$$

The response of yarn volume to a change in ρ_i is determined by geometry and is simply

$$\frac{\partial V}{\partial \delta_i} = \sum_{e=1}^{N_y} \frac{\pi l_e}{4} \tag{11}$$

If the objective was truly linear in δ, we could solve for the new design variables in a single step using the method of Lagrange multipliers

$$\begin{aligned} \delta_i^{\text{new}} &= \delta_i B_i^{\eta} \\ B_i &= -\frac{\dfrac{\partial c}{\partial \delta_i}}{\lambda \dfrac{\partial V}{\partial \delta_i}} \end{aligned} \tag{12}$$

However, to maintain careful treatment of the remaining nonlinearity in Eq. (10), the total change in diameter is limited to a step change in diameter (usually <5% of the initial diameter). Let m be the maximum step change of δ_i, and $\eta = 1/2$ be the numeric damping coefficient. The update scheme is summarized

$$\rho_i^{\text{new}} = \left\{\begin{array}{c} \text{if } \ \delta_i B_i^{\eta} \le \max(\delta_{\min}, \delta_i - m): \\ \max(\delta_{\min}, \delta_i - m) \\ \text{if } \ \max(\delta_{\min}, \delta_i - m) < \delta_i B_i^{\eta} < \min(1, \delta_i + m): \\ \delta_i B_i^{\eta} \\ \text{if } \ \delta_i B_i^{\eta} \ge \min(1, \delta_i + m): \\ \min(1, \delta_i + m) \end{array}\right\} \tag{13}$$

An additional inherent manufacturing limitation is in the braiding process itself; because braider yarns are in tension during the braiding process, a uniform structure is not created unless the clockwise and counterclockwise tensions are nearly equivalent. A remedy for this is to always match the number of warp and weft carriers, such that they carry the tension in opposite directions and thus balance the braid. To consider this effect, the optimization solver is commanded to group pairs of warp and weft yarns such that their diameters remain the same [22]. By grouping the average sensitivity (10) of the two yarns, they are forced to update equally (12).

While open-architecture lattices themselves will improve the buckling resistance of thin-walled structures they replace, this optimization method does not include buckling constraints. The

Table 4 Comparison of designed optimal braided lattice predicted properties to equivalent weight-per-length (~1.5 g/cm length) thin-walled commercial tubes

	Mass per unit length (g/cm)	Specific properties (per mass-per-length) Axial AEl/m (kN m/kg)	Torsion JGl/m (N m^3/kg)	Bending EIl/m (N m^3/kg)	Optimal structure characteristics No. of axials (mean diameter mm)	No. of helicals (mean diameter mm)	Helix angle (deg)
AL 6061 (analytical)	1.489	20.56	183.4	243.0			
Roll-wrapped CF (experimental)	1.018	26.44	409.6	2050			
Braided lattice (experimental, nonoptimal geometry)	1.200	10.17	319.9	115.3	8 (2.3)	8 (2.3)	45
Braided lattice (analysis, nonoptimal geometry)	1.205	10.19	297.1	115.9	8 (2.3)	8 (2.3)	45
Optimal strut (validated analysis)	0.996	62.56			16 (2.30)	4 (1.05)	45
Optimal driveshaft (validated analysis)	1.000		1362.9		0 (N/A)	32 (1.46)	44
Optimal boom (validated analysis)	0.997			4488.7	10 (2.00)	12 (1.7)	51

lattice structure is subject to several forms of buckling: Euler buckling of the entire structure, buckling of the individual yarns, and microscopic buckling of the CFs within the yarns. Typically this is not a problem since the length-to-diameter ratios at which carbon yarns buckle is usually long compared to the distance between interlaced joints in these structures [4]. To address this, an additional constraint on the optimization could be added, which limits the free length between bonded joint intersections to remain below a known critical length-to-diameter ratio. Our results here focus on the linear, small deflection stiffness of the structures, and do not consider these or other failure modes.

Results

Example applications of the optimization technique are shown for some common loading scenarios: axial compression (strut or column), torsion (driveshaft), cantilever bending (boom), and three-point bending (bridge). The baseline and final configuration for the optimization uses the same conditions shown in Table 2. The target volume fraction ν is 27% of the initial volume. Geometry and specific stiffness results are tabulated in Table 4.

A primary application of optimal braided lattice may be in the creation of axially loaded columns and struts in space frames. It would be expected that the ideal strut would consist of mostly axial reinforcement; indeed this result was found (Fig. 6(*a*)). Note that not all helical yarns were removed: reduction of the target volume to 25% would eliminate helical yarns entirely, and only the 16 evenly sized axial yarns would remain. The results with the fine helical yarns are shown to illustrate the (more practical) intermediate solution. All axial yarns are of equal size. A fine mesh of helical yarns helps contain them (and, practically, stabilizes the structure against buckling). By making the helical yarns as small as possible, not only is their weight decreased but the axial yarns maintain straighter paths (less undulation) along the structure.

The ideal torsional shaft (Fig. 6(*b*)) is also mostly intuitive: helical yarns carry the load along their axis more efficiently than axial yarns in the interlaced structure. Again, all the final yarns are of equal diameter. The final helix angle of 44 deg is explained by the fact that it allows yarns to carry internal loads along their axes. It is notable that in this loading scenario the solution converges toward a "smooth-walled" structure; in cases where the stress is uniform through the part, a lattice structure is nonoptimal unless buckling is considered, where low wall-thickness could cause a shell buckling instability.

Cantilever bending optimization results yield radical insight into design (Fig. 6(*c*)). First, the upper and lower axial yarns are maintained at full size. While it is doubtful that the idea of area moment of inertia can be directly applied to a truss structure that lacks a solid cross section, the increase in diameter and distance of structural material from the structure centerline certainly increases the stiffness. The real insight is that some helical yarns in the optimal braided lattice must be maintained to carry shear loads and to largely put the upper and lower axials into internal tensile and compressive loads rather than bending. The cantilever optimal braided lattice is more efficient with a shallow helix angle (large pitch), related to the ability to transfer the applied load into axial stresses in the upper and lower yarns.

Finally, a three-point bending loaded structure is optimized (Fig. 6(*d*)). While the large upper and lower axials are maintained, there is a much higher reliance on the helical yarns to carry shear. This is simply a feature of the length of the beam used (compared to the cantilever case).

Discussion

The intent of the framework developed here is to create tools for optimal braided lattice design. The design process combines

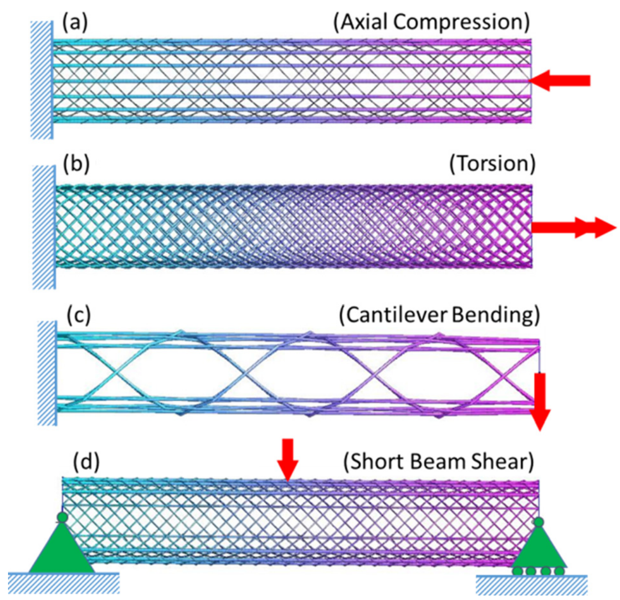

Fig. 6 Optimal braided lattice geometries: (*a*) optimal strut, (*b*) optimal driveshaft, (*c*) optimal boom, and (*d*) optimal bridge

careful representation of the braid geometry with a lightweight mechanical model and a fast optimization procedure.

From each step of the design process (geometry, analysis, and optimization), key design concepts for braided lattice design have been discovered. The first heuristic of design is that the diameter should always be increased to the limit of the application's space constraints. This increases the distance of yarns from the neutral axis and (for a given weight) will have less undulation between the yarns (as the ratio of mandrel diameter to yarn diameter increases). Helix angle is successfully determined by unconstrained parameter minimization. Yarn diameters are, as demonstrated, efficiently determined using optimality. Yarn locations also play a role in stiffness: Axial reinforcement is helpful with any axial stress (whether due to axial or bending loads). The helical yarns vary in the way they assist the structure; sometimes they carry loads directly as in torsional loading of the structure, and other times they transfer load from one set of axial yarns to another as in cantilever bending. Because truly optimal designs are often not directly intuitive, the optimization has achieved its goal of yielding insight into optimal braided lattice design.

The effectiveness of optimal braided lattices compared to suboptimal braided lattices is evaluated by comparing the specific stiffness of optimal and suboptimal geometries, as shown in Table 4. Suboptimal tubes clearly make poor use of material: 40% more carbon is used in helical yarns than in axial yarn despite the fact that it is primarily the axial yarns which contribute most to stiffness (except in torsional loading). Also, increasing diameter exponentially improves torsional and bending stiffness as the moment of inertia grows rapidly when diameter is increased. By designing optimal tubes using the methods described above, stiffness was increased 4.7 times for axial loading, 4.6 times for torsion, and 39.5 times for bending.

The effectiveness of optimal braided lattice as a designed structure is likewise evaluated by comparing the specific stiffness of standard commercially available tubular shapes to optimal braided lattice in Table 4. Thin-walled tubes become impractical below a limiting wall thickness due to structural weakness and perhaps manufacturing limitations, which is clearly seen in the range of available commercial tubes [4]. All tubes in Table 4 were chosen to have approximately equal weight per unit length (slightly less than 1.5 g/cm). This limits the diameter of the commercial tubes to below 2.5 cm, whereas the optimal braided lattice structures are all 3.18 cm diameter. This may initially sound like an unfair comparison (especially in bending and torsion), but that advantage is a key feature of the optimal braided lattice, i.e., its ability to increase diameter without a significant increase in mass. The aluminum 6061 tube is the largest diameter commercially available tube weighing less than 1.5 g/cm; the stiffness for that tube was computed using known material properties. The smooth-walled roll-wrapped CF tube is also the largest diameter commercially available tube that weighs less than 1.5 g/cm; the data for that tube were measured. The data in Table 4 confirm that optimal braided lattice designed tubes will dominate traditional thin-walled aluminum and CF tubes in all loading conditions besides uniaxial compression. In this linear stiffness comparison, the material choice determines AE—so the braided lattice has no advantage over another composite tube (until failure due to buckling is considered). However, for CF and aluminum, it is 3.33 and 7.43 times stiffer in torsion, respectively, and 2.19 and 18.47 times stiffer in bending, respectively.

Conclusion

A design process for the creation of optimal braided lattices was developed. The simulations from the very start have kept the constraints of maypole braiding machines in their construction. The combination of a geometry simulation, FEA tools, and a topological optimization method completes the required design stages. Techniques have accurately represented the composite yarns present in the structures. The simulation was validated and found to be an accurate predictor of actual optimal braided lattice tube stiffness. Using a compliance-based optimization method allows rapid establishment of the most efficient optimal braided lattice geometries. Future research will evaluate the strength properties of optimal braided lattice—particularly related to buckling resistance, where the unique geometry offers significant advantages where thin-walled tubes are susceptible to shell buckling and failure under concentrated (point) radial loading. The design tools developed herein show the potential gains made with braided truss composites. The methods are easily accessible to any engineer and can clearly improve the speed and accuracy with which open-structure tubes will be designed.

Acknowledgment

The authors would like to thank Highland Industries for supplying materials and expertise in physical testing. This work was supported by Highland Industry Composites Group, National Aeronautics and Space Administration Marshall Space Flight Center (NASA MSFC) Trade Study SLS-ADO-NNM14ZPS001, and NASA Alabama Space Grant Consortium (ASGC) Training Grant No. NNX10AJ80H.

Nomenclature

$c(\rho)$ = compliance, external energy
e = counts the elements along a yarn from 1 to N_y
i = counts the yarns from 1 to N_s
k = element stiffness matrix
m = optimization iteration step size
N_s = remaining number of yarns in the structure
N_y = number of elements within a yarn
u = element deformation vector
V_0 = the initial volume
$V(\rho)$ = the remaining structure volume
δ = design variable (an individual yarn's diameter squared, Δ^2)
$\boldsymbol{\delta}$ = vector of design variables (yarn-diameters-squared, Δ^2)
η = numeric damping coefficient
ν = a specified target volume fraction

References

[1] Popper, P., 1992, "Braiding," *Handbook of Composite Reinforcement*, S. M. Lee, ed., Wiley-VCH, New York, pp. 24–41.
[2] Jensen, D., Davis, K., Gunnel, B., Larson, G., Blunck, D., Evans, T., Hansen, S., Rogers, S., Boyce, J., Pate, E., and Ayers, J., III, 2009, "Apparatus, System, and Method for Filamentary Composite Lattice Structure Manufacturing," U.S. Patent US20090193961 A1.
[3] Freitas, G., Campbell, T., and Kasten, G., 2003, "Continuous Intersecting Braided Composite Structure and Method of Making Same," U.S. Patent US6647852 B1.
[4] Branscomb, D., 2012, "Minimal Weight Composites Utilizing Advanced Manufacturing Techniques," Ph.D. thesis, Auburn University, Auburn, AL.
[5] Ashby, M., 2005, *Materials Selection in Mechanical Design*, Elsevier Butterworth-Heinemann, Oxford, UK.
[6] Branscomb, D., Beale, D., and Broughton, R., 2013, "New Directions in Braiding," J. Eng. Fibers Fabr., **8**(2), pp. 11–24.
[7] Ko, F., Pastore, C., and Head, A., 1989, *Atkins and Pearce Handbook of Industrial Braiding*, Atkins and Pearce, Covington, KY.
[8] Du, G. W., and Popper, P., 1994, "Analysis of a Circular Braiding Process for Complex Shapes," J. Text. Inst., **85**(3), pp. 316–337.
[9] Zhang, Q., Beale, D., and Broughton, R. M., 1999, "Analysis of Circular Braiding Process, Part 1: Theoretical Investigation of Kinematics of the Circular Braiding Process," ASME J. Manuf. Sci. Eng., **121**(3), pp. 345–350.
[10] Akkerman, R., and Rodriguez, B. H., 2007, "Braiding Simulation and Slip Evaluation for Arbitrary Mandrels," 10th International ESAFORM Conference on Material Forming, Zaragoza, Spain, Apr. 18–20, pp. 1074–1079.
[11] Pickett, A., Sirtautas, J., and Erber, A., 2009, "Braiding Simulation and Prediction of Mechanical Properties," Appl. Compos. Mater., **16**(6), pp. 345–364.
[12] Durville, D., 2012, "Contact-Friction Modeling Within Elastic Beam Assemblies: An Application to Knot Tightening," Comput. Mech., **49**(6), pp. 687–707.
[13] Schneider, M., Pickett, A. K., and Wulfhorst, B., 2000, "A New Rotary Braiding Machine and CAE Procedures to Produce Efficient 3D-Braided Textiles for Composites," 45th International SAMPE Symposium and Exhibition, Long Beach, CA, May 21–25, pp. 266–276.
[14] Cook, R., Malkus, D., Plesha, M., and Witt, R., 2002, *Concepts and Applications of Finite Element Analysis*, Wiley, Madison, WI.

[15] Przemieniecki, J., 1968, *Theory of Matrix Structural Analysis*, McGraw-Hill, New York.
[16] Weaver, W., and Gere, J., 1990, *Matrix Analysis of Framed Structures*, 3rd ed., Van Nostrand Reinhold, New York.
[17] Lan, T. T., 2005, "Space Frame Structures," *Handbook of Structural Engineering*, CRC Press, Boca Raton, FL, pp. 24.1–24.50.
[18] Arora, J., 1989, *Introduction to Optimum Design*, McGraw-Hill, New York.
[19] Bendsoe, M., and Sigmund, O., 2003, *Topology Optimization—Theory, Methods, and Applications*, Springer, Berlin.
[20] Haftka, R. T., Gurdel, Z., and Kamat, M. P., 1990, *Elements of Structural Optimization*, Kluwer Academic Publishers, Boston.
[21] Kothari, N., 2014, "Mechanical Characterization of the Braided Composite Yarn and Bond Strength Evaluation of the Joints of the Open-Architecture Composite Structure (O-ACS)," M.S. thesis, Auburn University, Auburn, AL.
[22] Gurley, A., 2014, "Design and Analysis of Optimal Braided Composite Lattice Structures," Master's thesis, Auburn University, Auburn, AL.
[23] Rozvany, G. I. N., 2009, "A Critical Review of Established Methods of Structural Topology Optimization," Struct. Multidiscip. Optim., **37**(3), pp. 217–237.